Title

A Higher-Order Embedded Boundary Method for Time-Dependent Simulation of Hyperbolic Conservation Laws

Authors

Modiano, D

Colella, P

Publication Date

2000-03-01

LBNL-45239

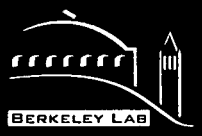

ERNEST ORLANDO LAWRENCE
BERKELEY NATIONAL LABORATORY

A Higher-Order Embedded Boundary Method for Time-Dependent Simulation of Hyperbolic Conservation Laws

D. Modiano and P. Colella

National Energy Research Scientific Computing Division

March 2000

To be presented at the *ASME 2000 Fluids Engineering Division Summer Meeting*, Boston, MA, June 11–15, 2000, and to be published in the Proceedings

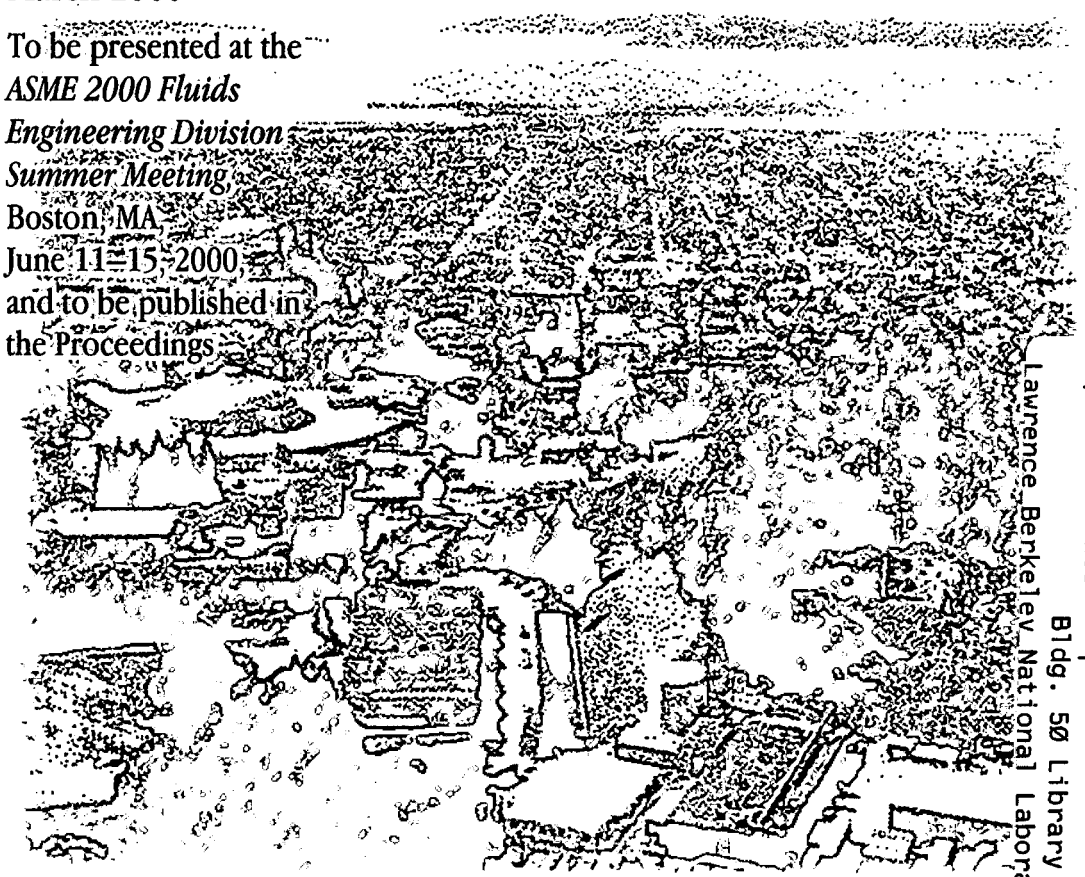

DISCLAIMER

LBNL-45239

A Higher-Order Embedded Boundary Method for Time-Dependent Simulation of Hyperbolic Conservation Laws

D. Modiano and P. Colella

National Energy Research Scientific Computing Division
Ernest Orlando Lawrence Berkeley National Laboratory
University of California
Berkeley, California 94720

March 2000

This work was supported by the Director, Office of Science, Office of Advanced Scientific Computing Research, Mathematical, Information, and Computational Sciences Division, of the U.S. Department of Energy under Contract No. DE-AC03-76SF00098.

A Higher-Order Embedded Boundary Method for Time-Dependent Simulation of Hyperbolic Conservation Laws

D. Modiano and P. Colella
Lawrence Berkeley National Laboratory
Berkeley, California 94720

March 2, 2000

Abstract

We present a new method for time-dependent simulation of hyperbolic conservation laws using a background Cartesian grid with an embedded boundary to represent geometry. The fluxes are produced at the centers of the regular grid cell faces by a Godunov method. Since the accuracy of the flux divergence depends on the fluxes consistently centered at the centroids of the irregular faces, we linearly interpolate the fluxes from the regular face centers to the irregular face centroids. We compare to an exact solution the propagation of a planar wave in a straight-walled channel inclined 30 degrees to the grid. The inconsistent flux method converges at well below first order in the irregular cells, and at about first order in the full domain. The present method, with consistent fluxes, converges at between first and second order in the irregular cells, and at second order in the full domain.

Nomenclature

A^x, A^y	flux Jacobian matrices, $\partial F^x/\partial U$ and $\partial F^y/\partial U$
F^x, F^y	flux vectors
F^B_{ij}	flux evaluated at centroid of embedded boundary segment
$F^x_{i+12,j}$, *etc.*	flux evaluated at centroid of irregular face
$\widetilde{F}^x_{i+12,j}$, *etc.*	flux evaluated at center of regular grid face
$\mathcal{L}$	exact hyperbolic evolution operator
L	discrete hyperbolic evolution operator
L^C	conservative discrete hyperbolic evolution operator
L^{NC}	nonconservative discrete hyperbolic evolution operator
U	numerical approximation to V
U^C	conservative numerical approximation to V
U^{NC}	reference state, nonconservative numerical approximation to V
U^P	preliminary update
V	exact solution to hyperbolic evolution equation
e	numerical error $U - V$
h	grid spacing
$\ell_{i+\frac{1}{2},j}$, $\ell_{i,j+\frac{1}{2}}$	area fraction of irregular face
ℓ^B_{ij}	area fraction of embedded boundary segment
$\ell^\infty(\cdot)$	max-norm of quantity
$\ell^2(\cdot)$	ℓ^2 norm of quanitity in entire solution domain
$\ell^2_{EB}(\cdot)$	ℓ^2 norm of quanitity in irregular cells
$\hat{n}^B_{ij}$	normal direction of embedded boundary segment
p	pressure
$p^\star$	pressure, solution to Riemann problem
u,v	x- and y-velocities
$\overline{x}_{i,j+\frac{1}{2}}$, $\overline{y}_{i+\frac{1}{2},j}$	fractional location of centroid of irregular face
$\overline{x}^B_{i,j}$, $\overline{y}^B_{i,j}$	fractional location of centroid of embedded boundary segment
$w_{lm,ij}$	redistribution weights
Δt	time step
Λ_{ij}	volume fraction of irregular cell
δM_{ij}	local volume-integrated conservation error of preliminary update
$\delta U_{lm,ij}$	redistribution increment
η_{ij}	interpolation coefficient for preliminary update
ρ	density
τ_{ij}	local truncation error

1 GOVERNING EQUATIONS

The governing equation is a two-dimensional hyperbolic system of conservation laws

$$\frac{\partial V}{\partial t} = -\nabla \cdot F(V) = -\frac{\partial F^x(V)}{\partial x} - \frac{\partial F^y(V)}{\partial y} \tag{1}$$

specialized to the equations of inviscid isentropic gas dynamics, with state vector $V = (\rho, \rho u, \rho v)^T$, and flux vectors $F^x = (\rho u, \rho u^2 + p, \rho uv)^T$ and $F^y = (\rho v, \rho uv, \rho v^2 + p)^T$ where ρ is the fluid density, u and v the x- and y-components of velocity, and $p = p_{\text{ref}}(\rho/\rho_{\text{ref}})^\gamma$ is the pressure.

2 NUMERICAL METHOD

The method presented here is based on a discretization of a complex problem domain as a background Cartesian grid with an embedded boundary representing the irregular domain region. See figure 1. We recognize three types of grid cells or faces: a cell or face that the embedded boundary intersects is *irregular*. A cell or face in the irregular problem domain which the boundary does not intersect is *regular*. A cell or face outside the problem domain is *covered*. The boundary of a cell is considered to be part of the cell, so that cells A, B and C in figure 2 are irregular. At the regular cells we use a numerical method designed for a uniformly spaced Cartesian grid with unit aspect ratio. We defer discussion of that method to section 2.5.1. At the irregular cells we use a conservative method based on finite volumes, described in this section.

State variables are defined at the geometric centers of the regular grid cells, even if a cell is irregular, and even if the center is outside the irregular domain. This is to enable the cancellation of error terms that results from the use of regular finite difference formulas. Cell centers have integer indices such as (i, j). Variables that are defined at the faces of cells are at the centers of the regular grid faces unless otherwise specified. Cell faces have mixed integer and half-integer indices, such as $(i + \frac{1}{2}, j)$ which is normal to x, and $(i, j + \frac{1}{2})$ which is normal to y.

An irregular cell is formed from the intersection of a grid cell and the irregular problem domain. We represent the segment of the embedded boundary as a single flat segment. Quantities located at the irregular boundary are given the superscript B. Depending on which grid faces the embedded boundary face intersects, the irregular cell can be a pentagon, a trapezoid, or a triangle, as shown in figure 3. A cell has a volume Λh^2, where Λ is its volume fraction. A face has an area ℓh, where ℓ is its area fraction. The polygonal representation is reconstructed from the volume and area fractions under the assumption that the cell has one of the shapes above. Since the boundary segment is reconstructed solely from data local to the cell, it will typically not be continuous

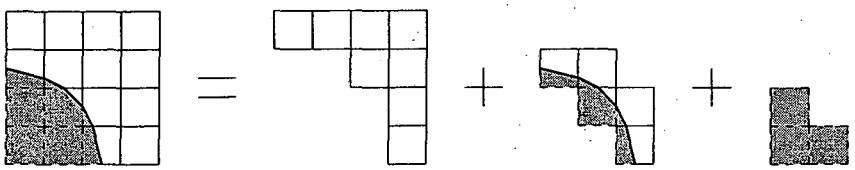

Figure 1: Decomposition of the grid into regular, irregular and covered cells. The gray regions are outside the solution domain.

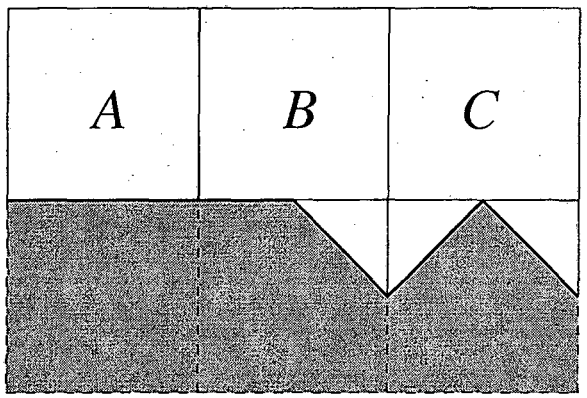

Figure 2: Cells with unit volume fraction that are irregular.

with the boundary segment in neighboring cells. We also derive the normal to the embedded boundary face $\hat{n}$ and the area of that face $\ell^B h$.

We do not represent irregular cells such as shown in figure 4, in which the embedded boundary has two disjoint segments in the cell. If such a cell is present, it will be reconstructed incorrectly.

The mathematical formulation and its implementation allow multiple irregular cells in one grid cell, such as seen in figure 5. However, for clarity of notation, references to irregular cells in this paper are as if there is only one irregular cell in any grid cell.

2.1 Conservative flux divergence

The central idiom for the solution method in irregular cells is that the quantity we are trying to compute is the cell-centered divergence of a field discretely specified at the cell faces. See figure 6. In this case we solve for U, an approximation to the exact solution V, by discretizing the exact hyperbolic evolution equation

$$\frac{\partial V}{\partial t} = -\nabla \cdot \vec{F}(V) = \mathcal{L}(V) \tag{2}$$

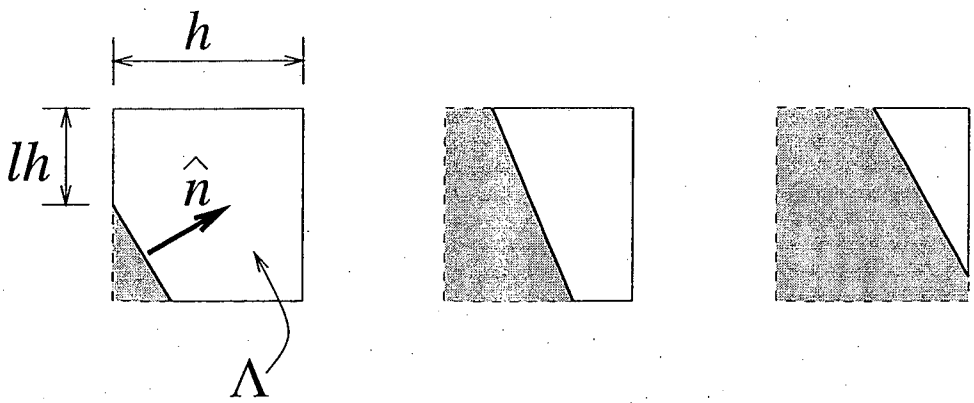

Figure 3: Representable irregular cell geometry. The gray regions are outside the solution domain.

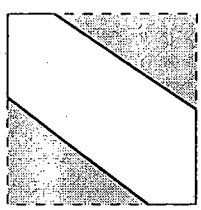

Figure 4: Unrepresentable irregular cell geometry. The gray region is outside the solution domain.

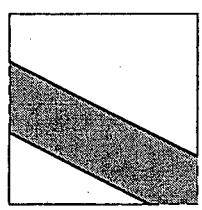

Figure 5: Multiple irregular cells sharing a grid cell. The left face of the grid cell is also multi-valued. The gray region is outside the irregular domain.

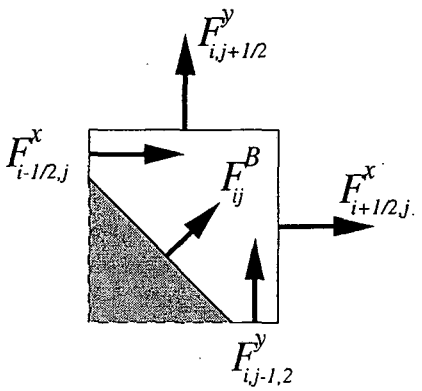

Figure 6: Flux divergence at an irregular cell.

in a finite volume manner to produce

$$\frac{U_{ij}^{n+1} - U_{ij}^{n}}{\Delta t} - L(U) = \frac{\partial V}{\partial t} - \mathcal{L}(V) + O(\Delta t + h) \tag{3}$$

in which $L(U) = D \cdot \vec{F}(U)$ where D is a discrete divergence operator. We are concerned with a conservative flux divergence

$$\begin{aligned} L^C(U) &= \mathcal{L}(V) + O(h/\Lambda) \\ &= -\frac{1}{\Lambda_{ij} h} \left(\ell_{i+\frac{1}{2},j} F^x_{i+\frac{1}{2},j} - \ell_{i-\frac{1}{2},j} F^x_{i-\frac{1}{2},j} \right. \\ &\quad \left. + \ell_{i,j+\frac{1}{2}} F^y_{i,j+\frac{1}{2}} - \ell_{i,j-\frac{1}{2}} F^y_{i,j-\frac{1}{2}} - \ell^B_{ij} F^B_{ij} \right). \end{aligned} \tag{4}$$

We can construct a scheme using the conservative update

$$U_{ij}^{n+1} = U_{ij}^{C} = U_{ij}^{n} + \Delta t L_{ij}^{C}. \tag{5}$$

This scheme would be unsatisfactory for reasons of accuracy and stability, as explained below.

2.2 Consistent discretization

Johansen and Colella [Johansen and Colella,1998] noted that the discrete divergence operator 4 is based on trapezoidal integration around the polygonal boundary of the irregular cell, which will be second-order accurate only if the fluxes F^x, F^y and F^B are consistently centered at the centroids of the irregular faces, whereas the fluxes are available at the centers of the regular grid faces, which in general will not coincide. In the context of solving elliptic

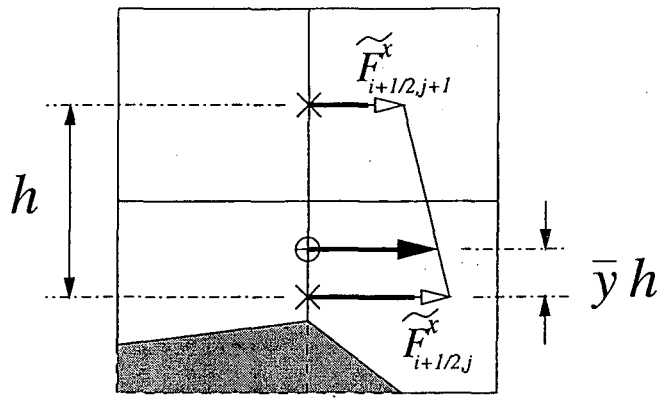

Figure 7: Flux interpolation from the grid face centers ($\times$) to the irregular face centroids ($\oplus$).

and parabolic problems, Johansen and Colella devised a method whereby the fluxes F^x and F^y are linearly interpolated from the regularly-centered faces to the irregularly-centered faces, providing a second-order accurate divergence (we defer until section 2.5.3 the details of computing F^B). We apply their method here. The interpolation formula for the case in figure 7 is

$$F^x_{i+\frac{1}{2},j} = \left(1 - \bar{y}_{i+\frac{1}{2},j}\right) \widetilde{F}^x_{i+\frac{1}{2},j} + \bar{y}_{i+\frac{1}{2},j} \widetilde{F}^x_{i+\frac{1}{2},j+1} \tag{6}$$

where $\widetilde{F}^x$ (or $\widetilde{F}^y$) are the fluxes centered at the regular faces and $\bar{y}h$ (or $\bar{x}h$ for faces oriented normal to y) is the distance from the regular face center to the irregular face centroid. This can also be written as

$$F^x_{i+\frac{1}{2},j} = \tfrac{1}{2}\left(1 + \ell_{i+\frac{1}{2},j}\right) \widetilde{F}^x_{i+\frac{1}{2},j} + \tfrac{1}{2}\left(1 - \ell_{i+\frac{1}{2},j}\right) \widetilde{F}^x_{i+\frac{1}{2},j+1}. \tag{7}$$

Interpolation of fluxes is only performed if the other face (at $(i+\frac{1}{2}, j+1)$ in the example) is regular. If it is not, we locally drop the order of accuracy and use the regular grid flux $\widetilde{F}^x_{i+\frac{1}{2},j}$ directly. We defer until section 2.5.1 the details of computing $\widetilde{F}$.

2.3 Preliminary update

A scheme using the conservative update of equation 5 is unstable for fixed Courant number $\Delta t/h$ due to the presence of Λ_{ij}, which may be arbitrarily small, in the denominator of the discrete flux divergence, equation 4. We use a redistribution scheme, originally developed for shock tracking [Chern and Colella,1987,

Bell, Colella, Welcome, 1991], to transfer unacceptably large changes in state from small cells to their neighbors.

Our redistribution method defines two updates, the unstable conservative update of equation 5 and a nonconservative *reference state*

$$U_{ij}^{NC} = U_{ij}^{n} + \Delta t L^{NC}(U_{ij}) \tag{8}$$

that is stable independent of Λ_{ij}. We linearly combine the conservative update U^C and the nonconservative update U^{NC} to form the *preliminary update*

$$U_{ij}^{P} = \eta_{ij} U_{ij}^{C} + (1 - \eta_{ij}) U_{ij}^{NC} \tag{9}$$

where $0 \leq \eta_{ij} \leq 1$. If $\eta_{ij} = 1$ we recover the original conservative method.

The nonconservative discrete divergence must be consistent,

$$L^{NC}(V) = \mathcal{L}(V) + O(h) \tag{10}$$

uniformly in Λ, in order for the overall scheme to be first-order accurate in the irregular cells,

$$\tau_{ij} = \frac{V_{ij}^{n+1} - V_{ij}^{n}}{\Delta t} - L(V^n)_{ij} = O(h). \tag{11}$$

In section 2.5.4 we describe our method for producing a reference state that satisfies this requirement.

To determine a proper value of η_{ij}, we define the volume-integrated conservation error of the reference state

$$\delta M_{ij} = \Lambda_{ij} h^2 (U_{ij}^{C} - U_{ij}^{NC}) \tag{12}$$

and rewrite the preliminary update 9 as a correction to the reference state,

$$\begin{aligned} U_{ij}^{P} &= U^{NC} + \eta_{ij}(U_{ij}^{C} - U_{ij}^{NC}) \\ &= U_{ij}^{NC} + \frac{\eta_{ij}}{\Lambda_{ij} h^2} \delta M_{ij}. \end{aligned} \tag{13}$$

This suggests that $\eta/\Lambda = O(1)$ is a necessary condition for small-cell stability. We choose $\eta_{ij} = \Lambda_{ij}$.

2.4 Redistribution

The preliminary update is not globally conservative. The volume-integrated conservation error in cell (i, j) is

$$\Lambda_{ij} h^2 (U_{ij}^{C} - U_{ij}^{P}) = (1 - \Lambda_{ij}) \delta M_{ij} \tag{14}$$

which must be added to the solution in order for the overall method to be conservative. We distribute $(1 - \Lambda_{ij})\delta M_{ij}$ to a neighborhood of cells adjacent

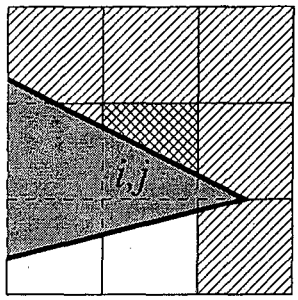

Figure 8: Redistribution neighborhood (diagonal lines) of cell (i, j) (crosshatching). Cells $(i-1, j-1)$ and $(i, j-1)$ (white) are excluded because they cannot be reached by monotone paths. Note that cells $(i, j+1)$ and $(i+1, j+1)$ are regular.

to (i, j) (including diagonally) which can be reached from it by a monotone path, *i.e.* without going around 180° corners. Some of these cells may be regular. See figure 8. We include the cell (i, j) in its own neighborhood. The state of a target cell is incremented by

$$\delta U_{lm,ij} = w_{lm,ij} \frac{1 - \Lambda_{ij}}{\Lambda_{lm} h^2} \delta M_{ij}. \tag{15}$$

The weights $w_{lm,ij}$ must satisfy

$$\frac{1}{\Lambda_{lm}} \sum_{(l,m) \in \mathrm{nbh}(i,j)} w_{lm,ij} = 1 \tag{16}$$

for the redistribution to be conservative, and

$$w_{lm,ij} = O(\Lambda_{lm}) \tag{17}$$

so that δU_{ij} is finite for small Λ_{lm}. For volume-weighted redistribution the weights are

$$w_{lm,ij} = \frac{\Lambda_{lm}}{\sum_{(i',j') \in \mathrm{nbh}(i,j)} \Lambda_{i',j'}}. \tag{18}$$

The redistribution update will satisfy

$$\delta U_{lm,ij} = O(h\, \Delta t) \tag{19}$$

which is the same order as $U^P - U^n$.

2.5 Godunov details

The numerical method is a multi-dimensional higher-order Godunov method based on the method described by Colella [Colella,1990] for general quadrilateral grids. The method presented here is restricted to Cartesian grids of a uniform mesh spacing h and unit aspect ratio. State variables are defined at the geometric centers of the regular grid cells, even if a cell is irregular, and even if the center is outside the irregular domain. This is to enable the cancellation of error terms that results from the use of regular finite difference formulas. Variables defined at the faces of cells are at the centers of the regular grid faces unless otherwise specified.

2.5.1 Regular Grid Method

The basic numerical method is a multi-dimensional higher-order Godunov method [Colella,1990]. An outline of the method follows. Cell centers have integer indices such as (i, j). Cell faces have mixed integer and half-integer indices, such as $(i + \frac{1}{2}, j)$ which is normal to x, and $(i, j + \frac{1}{2})$ which is normal to y.

1. Compute slopes. We compute the slopes of the state variables at the cell centers using the second-order central difference formula

$$\begin{aligned} \delta^x U_{ij} &= h\left(\frac{\partial U}{\partial x} + O(h^2)\right) \\ &= \tfrac{1}{2}\left(U^n_{i+1,j} - U^n_{i-1,j}\right) \end{aligned} \tag{20}$$

   at interior cells and a first-order one-sided difference formula such as

$$\begin{aligned} \delta^x U_{ij} &= h\left(\frac{\partial U}{\partial x} + O(h)\right) \\ &= U^n_{i+1,j} - U^n_{ij} \end{aligned} \tag{21}$$

   at cells adjacent to a boundary. The formulas for slopes in the y direction are similar.

2. Linearized normal extrapolation. Given data at the cell center (i, j) at time $t = n\Delta t$ we extrapolate to the left side of the face of the cell $(i+\frac{1}{2}, j)$ at time $t + \frac{1}{2}\Delta t = (n + \frac{1}{2})\Delta t$ as

$$U^L_{i+\frac{1}{2},j} = U^n_{ij} + \tfrac{1}{2}h\frac{\partial U}{\partial x} + \tfrac{1}{2}\Delta t\frac{\partial U}{\partial t}. \tag{22}$$

   Similarly, extrapolation to the right side of the face of the cell at $(i-\frac{1}{2}, j)$ is

$$U^R_{i-\frac{1}{2},j} = U^n_{ij} - \tfrac{1}{2}h\frac{\partial U}{\partial x} + \tfrac{1}{2}\Delta t\frac{\partial U}{\partial t}. \tag{23}$$

In order to approximate $\partial U/\partial t$, we linearize the conservative form of the equations

$$\frac{\partial U}{\partial t} = -\frac{\partial F^x}{\partial x} - \frac{\partial F^y}{\partial y} \tag{24}$$

in the x direction as

$$\frac{\partial U}{\partial t} = -A^x(U)\frac{\partial U}{\partial x} - \frac{\partial F^y}{\partial y} \tag{25}$$

so that

$$U^L_{i+\frac{1}{2},j} = U^n_{ij} + \tfrac{1}{2}h\frac{\partial U}{\partial x} - \tfrac{1}{2}\Delta t A^x_{ij}\frac{\partial U}{\partial x} - \tfrac{1}{2}\Delta t\frac{\partial F^y}{\partial y} \tag{26}$$

and

$$U^R_{i-\frac{1}{2},j} = U^n_{ij} - \tfrac{1}{2}h\frac{\partial U}{\partial x} - \tfrac{1}{2}\Delta t A^x_{ij}\frac{\partial U}{\partial x} - \tfrac{1}{2}\Delta t\frac{\partial F^y}{\partial y}. \tag{27}$$

We define $\widehat{U}^L_{i+\frac{1}{2},j}$ and $\widehat{U}^R_{i+\frac{1}{2},j}$ to be the result of the normal derivative term

$$\widehat{U}^L_{i+\frac{1}{2},j} = U^n_{ij} + \tfrac{1}{2}\left(1 - \frac{\Delta t}{h}A^x_{ij}\right)\delta^x U_{ij} \tag{28}$$

and

$$\widehat{U}^R_{i-\frac{1}{2},j} = U^n_{ij} - \tfrac{1}{2}\left(1 + \frac{\Delta t}{h}A^x_{ij}\right)\delta^x U_{ij}. \tag{29}$$

The formulas for extrapolation to the faces normal to the y direction are similar. Normal extrapolation must be completed for all sets of faces before transverse extrapolation can be done.

3. Transverse fluxes. With the definition of $\widehat{U}^L$ and $\widehat{U}^R$, the time-centered face states are computed as

$$U^L_{i+\frac{1}{2},j} = \widehat{U}^L_{i+\frac{1}{2},j} - \frac{\Delta t}{2h}\left(\widehat{F}^y_{i,j+\frac{1}{2},j} - \widehat{F}^y_{i,j-\frac{1}{2},j}\right) \tag{30}$$

and similarly for $U^R_{i-\frac{1}{2},j}$. We compute the transverse fluxes $\widehat{F}^y$ from the solution to the Riemann problem at each face defined by the states $\widehat{U}^L$ and $\widehat{U}^R$ at the face normal to y.

4. Riemann solution. We solve the Riemann problem defined by the left and right states U^L and U^R to yield a single time-centered value at each face $U^{n+\frac{1}{2}}$.

5. Flux difference. We compute the fluxes $\widetilde{F}^x$ and $\widetilde{F}^y$ at each face from the Riemann solution. The state vector is advanced by one time step by the flux difference,

$$U^{n+1}_{ij} = U^n_{ij} - \frac{\Delta t}{h}\left(\widetilde{F}^x_{i+\frac{1}{2},j} - \widetilde{F}^x_{i-\frac{1}{2},j} + \widetilde{F}^y_{i,j+\frac{1}{2}} - \widetilde{F}^y_{i,j-\frac{1}{2}}\right) \tag{31}$$

2.5.2 Irregular slopes

The computation of the slopes is modified if access to a cell needed by the central difference stencil is blocked by the irregular boundary (this does not only mean that a cell is outside the irregular domain; for an example, in figure 9, the irregular boundary blocks access to cell $(i+1, j)$ for a stencil centered at cell (i, j)). We use a one-sided second-order formula. For example, if cell $(i+1, j)$ is unavailable, the slope $\delta^x U_{ij}$ is computed as

$$\begin{aligned} \delta^x U_{ij} &= h\left(\frac{\partial U}{\partial x} + O(h^2)\right) \\ &= \tfrac{1}{2}\left(U_{i-2,j} - 4U_{i-1,j} + 3U_{ij}\right). \end{aligned} \tag{32}$$

If the cell $(i-2, j)$ is also unavailable, we use a first-order formula. If the cell $(i-1, j)$ is unavailable, the slope is set to zero. The latter is an indication that the geometry is under-resolved.

2.5.3 Embedded boundary flux

The embedded boundary flux F_{ij}^B is evaluated at the centroid of the embedded boundary face, which does not coincide with any of the regular grid faces. The entire Godunov procedure must be performed to evaluate this flux. The embedded boundary represents a solid wall, so there is no convective transport across it. Thus, the only non-zero flux is the pressure term of the momentum flux.

The slopes computed for the regular scheme can be reused. Since the embedded boundary is not, in general, aligned with the grid, there is no notion of normal and tangential grid directions for differencing. The predictor is similar to the normal stage of the regular grid predictor, except that spatial extrapolation is performed to the centroid of the embedded boundary face $(\bar{x}^B h, \bar{y}^B h)$ (measured relative to the center of the grid cell), which is arbitrary within the cell, and the derivatives are linearized in both grid directions. Thus,

$$\widehat{U}_{ij}^B = U_{ij}^n + \left(\bar{x}_{ij}^B - \frac{\Delta t}{2h} A_{ij}^x\right)\delta^x U_{ij} + \left(\bar{y}_{ij}^B - \frac{\Delta t}{2h} A_{ij}^y\right)\delta^y U_{ij}. \tag{33}$$

A Riemann problem must be solved at the embedded boundary face. Only one state is available. Since the embedded boundary represents a solid wall, an artificial state is constructed which is identical to $\widehat{U}_{ij}^B$ except the sign of the normal velocity is reversed. Recall that we only need to compute the pressure term, for the momentum flux. The solution to this Riemann problem is

$$p_{ij}^\star = \hat{p}_{ij}^B - \hat{u}_{ij}^B \hat{c}_{ij}^B \tag{34}$$

where u is the velocity normal to the embedded boundary and c is the speed of

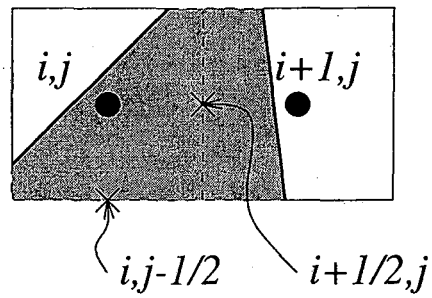

Figure 9: Double-valued extended face at $(i+\frac{1}{2}, j)$.

sound. The flux is then

$$F^B_{ij} = \begin{Bmatrix} 0 \\ p^*_{ij} n^x_{ij} \\ p^*_{ij} n^y_{ij} \\ 0 \end{Bmatrix} \tag{35}$$

2.5.4 Reference State

The reference state U^{NC} is a stable, nonconservative approximation to U^{n+1}. It is intended to resemble the finite difference scheme used on the regular grid, and does not include the effects of the geometry. Computation of the reference state differs from computation of the regular grid update when a face required for the flux difference is outside the valid irregular domain. These faces are called *extended faces* and the quantities at them are called *extended states* and *extended fluxes*.

Extended values are specific to the cell they border. In figure 9, face $(i+\frac{1}{2}, j)$ has two sets of extended values, one for cell (i, j) and one for cell $(i+1, j)$. The implementation allows double-valued extended states, but for clarity of notation that is not reflected in this description.

Consider computation of the flux $\widetilde{F}^x_{i+\frac{1}{2},j}$ for cell (i, j) when the face $(i+\frac{1}{2}, j)$ is invalid. The left and right states needed for the solution of the Riemann problem are computed as follows. On the "inner" side of the face (L in this example) we extrapolate from the center of cell (i, j) using first-order one-sided slopes.

$$\widehat{U}^I_{i+\frac{1}{2},j} = U^n_{ij} + \tfrac{1}{2}\left(1 - \frac{\Delta t}{h} A^x_{ij}\right) \delta^x U_{ij} \tag{36}$$

where

$$\delta^x U_{ij} = U^n_{ij} - U^n_{i-1,j}. \tag{37}$$

On the "outer" side of the face, we extrapolate from the center of cell $(i-1, j)$

using first-order one-sided slopes computed from cells $(i-1,j)$ and $(i-2,j)$.

$$\widehat{U}^O_{i+\frac{1}{2},j} = U^n_{i-1,j} + \tfrac{1}{2}\left(3 - \frac{\Delta t}{h} A^x_{i-1,j}\right)\delta^x U_{i-1,j} \tag{38}$$

where

$$\delta^x U_{i-1,j} = U^n_{i-1,j} - U^n_{i-2,j}. \tag{39}$$

The Riemann problem is solved using the inner and outer states $\widehat{U}^I$ and $\widehat{U}^O$ defined above, in order to compute transverse fluxes $\widehat{F}^x$ and $\widehat{F}^y$. The transverse flux update is performed with the use of the extended fluxes. The extended states themselves are updated with the transverse flux.

$$\begin{aligned} U^I_{i+\frac{1}{2},j} &= \widehat{U}^I_{i+\frac{1}{2},j} - \frac{\Delta t}{2h}\left(\widehat{F}^y_{i,j+\frac{1}{2}} - \widehat{F}^y_{i,j-\frac{1}{2}}\right) \\ U^O_{i+\frac{1}{2},j} &= \widehat{U}^O_{i+\frac{1}{2},j} - \frac{\Delta t}{2h}\left(\widehat{F}^y_{i,j+\frac{1}{2}} - \widehat{F}^y_{i,j-\frac{1}{2}}\right) \end{aligned} \tag{40}$$

Note that it is possible for the transverse fluxes to be extended fluxes, as is $\widehat{F}^y_{i,j-\frac{1}{2}}$ in figure 9.

The fluxes $\widetilde{F}^x$ and $\widetilde{F}^y$ for computation of the reference state,

$$U^{NC}_{ij} = U^n_{ij} - \frac{\Delta t}{h}\left(\widetilde{F}^x_{i+\frac{1}{2},j} - \widetilde{F}^x_{i-\frac{1}{2},j} + \widetilde{F}^y_{i,j+\frac{1}{2}} - \widetilde{F}^y_{i,j-\frac{1}{2}}\right), \tag{41}$$

are computed from the solution of the Riemann problem defined by U^I and U^O. There is no influence of the embedded boundary on the reference state, and these fluxes are centered at the centers of the regular grid faces.

3 TEST CASES

3.1 Simple wave exact solution

The simple wave defined here is the time-dependent exact solution of the straight-walled channel test case. The flow field is a stagnant fluid with a small perturbation in a single characteristic quantity. We specify an initial profile for density at time $t = 0$,

$$\rho_0(x) = \rho_{\text{ref}}\left(1 + \alpha f(\bar{x})\right) \tag{42}$$

where

$$f(\bar{x}) = \begin{cases} (\bar{x}^2 - 1)^4 & \text{if } 0 \le \bar{x} \le 1 \\ 0 & \text{otherwise} \end{cases} \tag{43}$$

with the dimensionless coordinate

$$\bar{x} = \vec{x}\cdot\hat{n}/w. \tag{44}$$

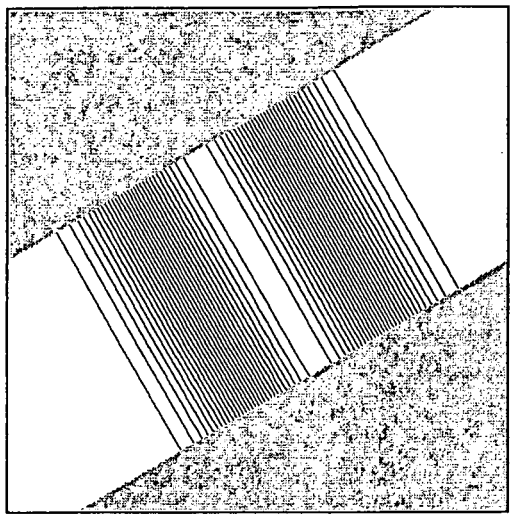

Figure 10: Initial condition for test problem. Density varies from 1.0 at the left and right to 1.001 in the center.

The parameters are α, the amplitude of the wave; w, the width of the wave; and $\hat{n}$, the direction of propagation of the wave. The initial pressure is found from the isentropic relation

$$\ln p_0(x) - \gamma \ln \rho_0(x) = \ln p_{\text{ref}} - \gamma \ln \rho_{\text{ref}}. \tag{45}$$

The initial fluid velocity is found by characteristic analysis. The value of the Riemann invariant

$$J_+ = u + \frac{2c}{\gamma - 1} \tag{46}$$

is taken from the profile $u = u_0(x)$, $c = c_0(x)$, while the Riemann invariant

$$J_- = u - \frac{2c}{\gamma - 1} \tag{47}$$

is taken from the reference ambient conditions $u = 0$, $c = c_{\text{ref}}$. Equating

$$u_0(x) = \tfrac{1}{2}\left(J_+ + J_-\right) \tag{48}$$

yields

$$u_0(x) = \frac{2}{\gamma - 1}\left(c_0(x) - c_{\text{ref}}\right) \tag{49}$$

The exact solution $u(x,t)$ is obtained by using the profile $u_0(x_+)$, $c_0(x_+)$ in equation 46, where $x_+(x,t) = x - (u + c)t$, and iterating to convergence of x_+.

3.2 Simple wave pulse in straight channel

The walls of the channel are angled 30° to the x-axis. The parameters of the pulse are $\alpha = 10^{-3}$, $w = 0.4$, and $\hat{n} = (\frac{1}{2}\sqrt{3}, \frac{1}{2})$. We used grids in the range $64 \times$

64 to 512 × 512. Each grid has irregular cells with a wide range of volume fraction. The solution error is calculated from the analytic exact solution of section 3.1. We compare the error, $e_{ij} = U_{ij} - V_{ij}$, of simulations using consistent fluxes to simulations using fluxes centered at the regular grid faces. Three error measures are shown: $\|e\|_\infty$, the maximum error; $\|e\|_{2,EB}$, the ℓ^2 norms of the field error in the irregular cells only; and $\|e\|_2$, the ℓ^2 norms of the field error in the entire problem domain. Tables 1–4 show the errors in density and x-momentum. The rate listed is the error exponent p for which the errors satisfy $e(h) = O(h^p)$. It is calculated as $p_n = \log_2 (\|e(2h)\|_n / \|e(h)\|_n)$. We expect $p = 1$ in the irregular cells for the consistent flux method. Since the irregular region is a set of points codimension one lower than the full domain, we expect an extra factor of h, or $p = 2$, for the full domain in the asymptotic limit.

The inconsistent flux method shows the maximum error and the irregular cells error norm to converge at well below first order, and the full domain error norms to converge at about first order. The present method, with consistent fluxes, shows the maximum error and the irregular cells error to converge at between first and second order, and the full domain error norm to converge at about second order. The convergence rates for x-momentum is significantly poorer than that for density, due to the convection of vorticity errors along the wall.

References

[Bell, Colella, Welcome, 1991] J. B. Bell, P. Colella and M. L. Welcome. "Conservative Front-Tracking for Inviscid Compressible Flow." AIAA paper 91-1599-CP, in *Proceedings, AIAA 10th Computational Fluid Dynamics Conference*. Honolulu, Hawaii, June 24–27, 1991, pp. 814–822.

[Chern and Colella,1987] I.-L. Chern and P. Colella. "A Conservative Front-Tracking Method for Hyperbolic Conservation Laws." UCRL-97200, Lawrence Livermore National Laboratory, 1987.

[Colella,1990] P. Colella. "Multidimensional Upwind Methods for Hyperbolic Conservation Laws." *Journal of Computational Physics*, 87:171–200, 1990.

[Johansen and Colella,1998] H. Johansen and P. Colella. "A Cartesian Grid Embedded Boundary Method for Poisson's Equation on Irregular Domains." *Journal of Computational Physics*, 147(1):60–85, November 1998.

[Pember,1995] R. B. Pember, J. B. Bell, P. Colella, W. Y. Crutchfield, and M. L. Welcome. "An Adaptive Cartesian Grid Method for Unsteady Compressible Flow in Irregular Regions." *Journal of Computational Physics*, 120:278–304, 1995.

Table 1: Errors and convergence rates of density for consistent flux scheme.

grid	$\|e\|_\infty$	p_∞	$\|e\|_{2,EB}$	$p_{2,EB}$	$\|e\|_2$	p_2
64×64	5.74(−6)	—	4.91(−7)	—	9.73(−8)	—
128×128	2.26(−6)	1.35	1.79(−7)	1.46	2.56(−8)	1.92
256×256	1.03(−6)	1.13	6.40(−8)	1.49	6.77(−9)	1.92
512×512	4.45(−7)	1.22	2.29(−8)	1.48	1.75(−9)	1.95

Table 2: Errors and convergence rates of x-momentum for consistent flux scheme.

grid	$\|e\|_\infty$	p_∞	$\|e\|_{2,EB}$	$p_{2,EB}$	$\|e\|_2$	p_2
64×64	7.86(−6)	—	6.56(−7)	—	1.27(−7)	—
128×128	3.48(−6)	1.35	2.95(−7)	1.15	4.06(−8)	1.65
256×256	1.67(−6)	1.06	1.25(−7)	1.24	1.23(−8)	1.72
512×512	7.84(−7)	1.09	5.05(−8)	1.31	3.57(−9)	1.78

Table 3: Errors and convergence rates of density for inconsistent flux scheme.

grid	$\|e\|_\infty$	p_∞	$\|e\|_{2,EB}$	$p_{2,EB}$	$\|e\|_2$	p_2
64×64	6.26(−6)	—	1.02(−6)	—	2.07(−7)	—
128×128	3.28(−6)	0.93	6.60(−7)	0.64	9.58(−8)	1.11
256×256	2.45(−6)	0.42	3.68(−7)	0.84	4.00(−8)	1.26
512×512	2.23(−6)	0.13	2.15(−7)	0.78	1.67(−8)	1.26

Table 4: Errors and convergence rates of x-momentum for inconsistent flux scheme.

grid	$\|e\|_\infty$	p_∞	$\|e\|_{2,EB}$	$p_{2,EB}$	$\|e\|_2$	p_2
64×64	6.26(−6)	—	9.22(−7)	—	1.83(−7)	—
128×128	4.31(−6)	0.85	6.29(−7)	0.55	8.92(−8)	1.03
256×256	4.04(−6)	0.10	4.74(−7)	0.41	4.98(−8)	0.84
512×512	4.66(−6)	-0.21	4.23(−7)	0.16	3.17(−8)	0.65

ERNEST ORLANDO LAWRENCE BERKELEY NATIONAL LABORATORY
ONE CYCLOTRON ROAD | BERKELEY, CALIFORNIA 94720

Prepared for the U.S. Department of Energy under Contract No. DE-AC03-76SF00098